Materials Chemistry Horizons

RESEARCH

Optimization of the Adsorption Performance of Tin Selenide Nanostructures Using Response Surface Methodology and Box–Behnken Design

Marzieh Khademalrasool [a,b,*], Elham Kharatzadeh [c,d], Atefeh Pourjahed [e]

[a] Department of Physics, Jundi-Shapur University of Technology, Dezful, Iran
[b] Jundi-Shapur Research Institute, Jundi-Shapur University of Technology, Dezful, Iran
[c] Department of Physics, Ahvaz Branch, Islamic Azad University, Ahvaz, Iran
[d] College of Skills and Entrepreneurship, Ahvaz Branch, Islamic Azad University, Ahvaz, Iran
[e] Department of Chemical Engineering, Jundi-Shapur University of Technology, Dezful, Iran

***Corresponding author**: mkhademalrasool@jsu.ac.ir, mkhademalrasool@yahoo.com (M. Khademalrasool)

Mater. Chem. Horizons, 2025, 4(1), 16-28 10.22128/mch.2026.3029.1068 OPEN ACCESS

ABSTRACT

In this study, the adsorption performance of tin selenide nanostructures was investigated as an efficient nano-adsorbent for the removal of methylene blue dye from aqueous solutions. Tin selenide nanostructures were synthesized using the co-precipitation method and characterized using Fourier transformation infrared spectroscopy, energy dispersive X-ray spectroscopy, Field emission scanning electron microscopy, Brunauer–Emmett–Teller method, and X-ray diffraction techniques to assess their physical and morphological properties. Adsorption parameters were optimized using response surface methodology based on the Box-Behnken model in Design Expert software. Optimal conditions for maximum dye removal were determined as pH 8, a contact time of 50 minutes, and an adsorbent mass of 0.0157 g. Kinetic studies revealed that the adsorption process followed the pseudo-second-order model (R^2= 0.99989) with an initial adsorption rate of 680.28 mg/L and equilibrium achieved in 10 minutes. Isotherm analysis showed consistency with both Langmuir and Freundlich models. The Langmuir model indicated a maximum adsorption capacity of 26.66 mg/g and a favorable equilibrium parameter (RL=0.16084). The Freundlich model confirmed the favorable and predominantly physical nature of the adsorption. These findings demonstrate the potential of tin selenide nanostructures as efficient and cost-effective adsorbents for dye removal, offering promising applications in environmental remediation.

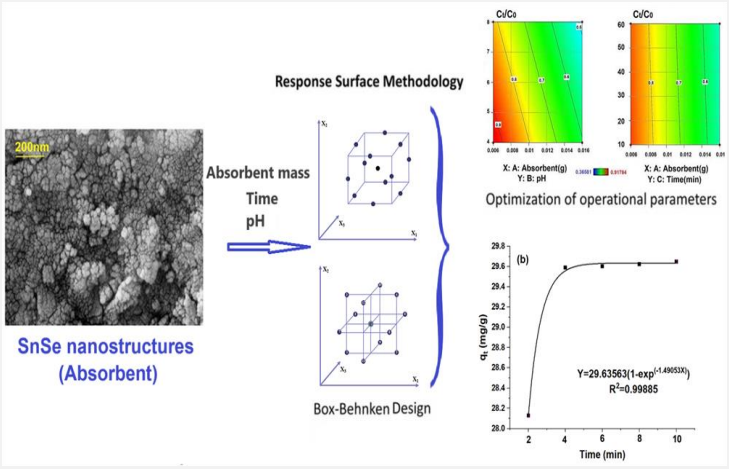

Keywords: SnSe nanostructure, aqueous environment, response surface methodology, adsorption, box-Behnken design

1. Introduction

Clean water is essential for both human life and key industries such as food production, textiles, automotive manufacturing, and furniture making. Population growth, agriculture, and industrial activities contribute to the wastewater contamination with dyes and other pollutants, thereby deteriorating water quality. These pollutions create significant environmental hazards and disrupt commercial activities. Furthermore, a significant portion of the global population depends on unsafe and unreliable drinking water sources due to limited water availability. As a result, the global need for water recycling and reuse is imperative, highlighting the importance of developing efficient and cost-effective methods for removing pollutants from wastewater. Water contaminants are classified into various groups including pathogens, chemical pollutants, hospital waste, nutrient pollutants, inorganic and organic pollutants. Dyes used in textiles, paints, and pigments are major water pollutants with over 100,000 commercial types. Exposure to

Received: August 26, 2025
Received in revised: January 01, 2026
Accepted: January 20, 2026
This is an open access article under the CC BY license

dyes can cause skin irritation, respiratory problems, and increased cancer risk. Some dyes are chemically and photolytically stable, preventing natural degradation [1, 2].

Effective removal of dyes from wastewater is crucial for safe discharge into natural water bodies. Various methods such as ion-exchange, precipitation, membrane filtration, electrochemical treatment, reverse osmosis, solvent extraction, and adsorption, are commonly used to remove dyes from wastewater, but adsorption is preferred for its flexibility, simplicity, low cost, and resistance to toxic pollutants. Adsorption also prevents the production of harmful byproducts, making it an effective treatment method. However, common adsorbents like activated carbon and agricultural solids are costly and less efficient due to their small particle size, resulting in longer times for contaminant removal. Therefore, there is an urgent need to develop cost-effective adsorbents with higher removal rates and better adsorption capacities. Nanostructured materials offer an innovative approach to water purification, with various types such as carbon-based materials (carbon nanotubes, carbon nanoparticle; etc), metal oxides (ZnO, MgO, CaO; etc), metal nanostructures (Au NPs, Ag NPs; etc), magnetic nanomaterials (Fe_2O_3, Fe_3O_4; etc), silicon nanomaterials, and metal chalcogenides (CuS, CuSe, MnS, MnSe; etc) are promising as nano-adsorbents [3-5]. Despite their rapid development, these materials are not yet commercially viable. The effective adsorption of dyes by nanostructures depends on factors such as electrical charge, surface area, and dye conformation. Therefore, ongoing research is focused on discovering new porous nanomaterials with high surface area, tunable morphology, and strong chemical and thermal stability. This study focuses on the use of tin selenide (SnSe) nanostructures, a type of metal-chalcogenide, for dye adsorption due to their unique properties such as high charge mobility, intrinsic defects, porosity, low thermal conductivity, high anisotropy, cheap, and low toxicity. The layered structure of SnSe, with covalent bonds within layers, Van der Waals interactions between layers, and surface vacancies, creates numerous adsorption sites, which significantly improves the adsorption efficiency [6-8]. In this study, for investigation of the adsorption performance of SnSe nanostructure as new nano-adsorbent in the aqueous media, initially, SnSe nanostructure was synthesized using the co-precipitation method. Then, the physical, surface, and morphological properties of the synthesized adsorbent were characterized using various techniques. In addition, to optimize dye adsorption, the effect of parameters such as pH, contact time, and adsorbent mass on the efficiency of the adsorbent in removing dye from aqueous solutions, response surface methodology (RSM) with the Box-Behnken design (BBD) is used. This approach minimizes experimental requirement and saves time and resources [9-11]. Since و no study has been reported on the optimization and modeling of SnSe chalcogenide nanostructure for methylene blue (MB) dye adsorption using the RSM approach, this study could be of interest to many researchers.

2. Materials and experimental procedure

2.1. Measurements

The structure, phase, and interactions between precursors and solvents were analyzed using X-ray diffraction (XRD) and Fourier transformation infrared spectroscopy (FT-IR). These measurements were recorded with a Philips-PW1730 X-ray instrument utilizing Cu-kα1 radiation (λ = 1.5406 Å) and a Bomem MB-series -102 FT-IR spectrometer, respectively. The Brunauer–Emmett–Teller (BET) method and Barrett– Joyner–Halenda (BJH) method were employed to analyze the specific surface area and pore structure of samples through N2 adsorption-desorption at liquid nitrogen temperature (77K), using a BEISORP MINI model instrument. The elemental concentration and morphology of the nanostructure were investigated using energy dispersive X-ray spectroscopy (EDX) and Field emission scanning electron microscopy (FE-SEM, TE-SCAN).

2.2. Synthesis of SnSe nanostructure

In order to prepare the SnSe nanostructure as an adsorbent, a certain amount of tin (II) chloride dehydrate ($SnCl_2.2H_2O$) (0.005 M) and selenium powder (0.005 M) were separately dissolved in 50 ml of deionized (DI) water for 15 min. Then, glycine amino acid (0.01g) and sodium borohydride (0.04917g) were added as the surfactant agents and reducing. All precursors used in our study were purchased from Sigma-Aldrich CO with a purity of 99.99%. Afterward, selenium in a reduced state was gradually introduced into the tin solution, and the mixture was stirred for

3 hours and then left for 24 hours to settle. The obtained product was then washed several times with DI water to remove impurities and dried at room temperature [7].

2.3. MB solution preparation and adsorption studies

In this study, the adsorption capacity of SnSe nanostructure was investigated by adsorption of the solution of the MB dye as a pollutant. The analysis was performed on a closed box in the dark using MB solutions prepared at a concentration of 10 ppm. All tests were continuously stirred at room temperature and after the end of the test time; all the samples were centrifuged to separate the suspended solids. Finally, a UV-Visible spectrophotometer was used to examine each sample. All tests were performed to evaluate the changes in three factors of pH, contact time, and adsorbent mass in 12 experiments. The adsorption capacity at equilibrium condition (q_e), the adsorption capacity at different times (q_t), and MB adsorption efficiency were calculated according to the equations (1), (2), and (3).

$$q_e = \frac{(C_0 - C_e)V}{m} \quad (1)$$

$$\text{Removal of MB}(\%) = \frac{C_0 - C_t}{C_0} \times 100\% \quad (2)$$

where C_0 (mgL^{-1}) is MB concentration at the initial condition (10 ppm), C_e is the equilibrium concentration (mg/L), C_t is MB concentration at different times, V(L) and m (g) are volume of MB solution and adsorbent mass [12].

2.4. Design of experiments and statistical analysis

In order to improve the experimental design, three distinct variables were identified as crucial factors that could have a substantial impact on the study results. These variables encompassed the adsorbent mass, pH levels, and the contact time between the adsorbent and the solution, with three levels shown in **Table 1**. To statistically identify the effective factors, Box-Behnken Design as a type of RSM, was done and effects of the factors were evaluated using the analysis of variance (ANOVA) method by Design Expert version 13 software. Contour plots were used to visually represent the effect of independent variables on dependent variables.

Table 1. Factors and their levels for design of experiments in Box-Behnken design.

Factors	Factor levels		
Adsorbent mass (g)	0.006	0.011	0.016
pH	4	6	8
Time (min)	10	35	60

3. Results and discussion

3.1. Characterization of SnSe nanostructure

Figure 1a shows the crystal structure of the SnSe nanostructure examined by XRD analysis. According to the standard card (JCPDS-00-14-0159), the nanostructure exhibits an orthorhombic SnSe phase. Three peaks were observed at approximately 2θ = 26.75°, 23.85°, and 34.10°, indicating the presence of impurity phases of tin (IV) oxide (SnO_2) and tin diselenide ($SnSe_2$). The formation of the SnO_2 phase may be due to the presence of oxygen during the synthesis process by the co-precipitation method. Since Sn ions exist in two oxidation states (Sn^{2+} and Sn4+) and have a high tendency to react with oxygen, both $SnSe_2$ and SnO_2 phases can be formed in the resulting nanostructure. Despite repeated attempts at synthesis, the resulting nanostructure consistently exhibited a mixed phase of SnSe, $SnSe_2$, and SnO_2. The presence of these excess Se_2- anions can enhance the adsorption efficiency with the MB cationic dye [13-15]. **Figure 1b** shows the FT-IR spectrum of the sample in the range of 500-3500 cm^{-1}. The peaks observed between 618 and 1117 cm^{-1} correspond to Sn-Se and B-H stretching vibrations, which are attributed to precursors such as $NaBH_4$ on the surface of the SnSe nanostructure. The adsorption bands in the range of 1281-1621 cm^{-1} are attributed to typical functional groups such as C–O, C=C, and C=O, which are due to the presence of the glycine amino acid ($C_2H_5NO_2$). In addition, the peak at 3411 cm^{-1} is related to the (O-H) stretching vibration of hydroxyl groups present in various functional groups, including aldehydes, alcohols, and acids [16, 17]. The textural characteristics and the pore size distribution of the SnSe nanostructure are shown in **Figure 1c** by the N_2 adsorption-desorption isotherm and BJH method. As can be seen, the hysteresis loop type of the prepared sample is H_2-type

hysteresis. The BJH analysis estimates the surface area, average pore diameter, and pore volume of the nanostructure to be 25.73 m^2/g, 10.75 nm, and 0.827 cm^3/g, respectively. These properties suggest that the nanostructure is mesoporous, which is beneficial for pollutant adsorption. **Figure 1e** and **f** show the morphology and standard EDX spectrum of the sample. The images show cracks between the nanoparticles that enhance dye adsorption and are consistent with the results of BET analysis. Furthermore, the EDX analysis shows that the Sn and Se are evenly distributed throughout the nanostructure [6, 18].

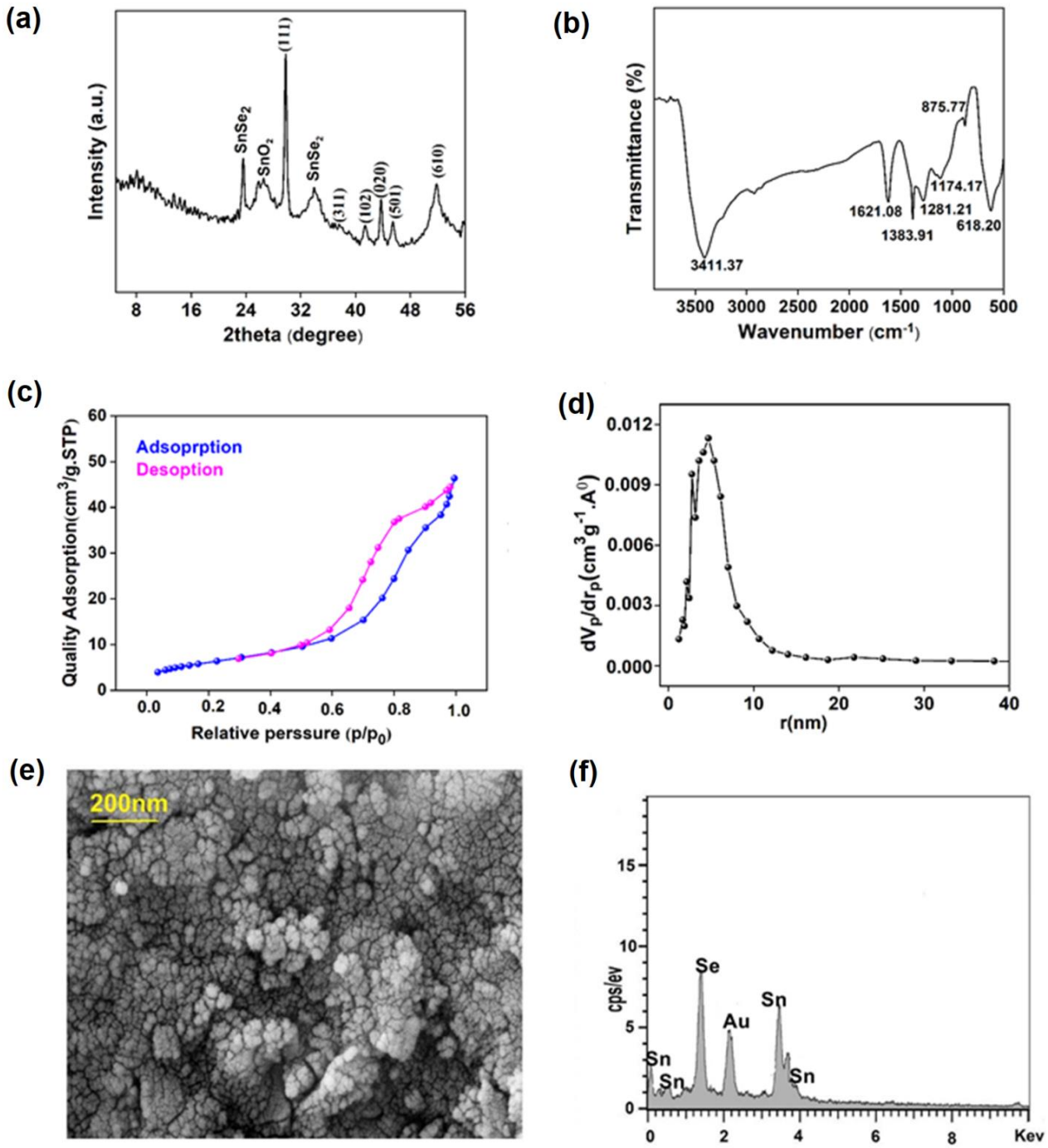

Figure 1. (**a**) XRD pattern, (**b**) FT-IR spectrum, (**c**) BET analysis, and (**d**) the pore-size distribution curve, (**e**) FESEM image, and (**f**) the standard EDX spectrum of synthesized SnSe nanostructure.

3.2. Statistical analysis of adsorption

The adsorption efficiency of the SnSe adsorbent for each of the designed experiments is shown in **Table 2.** The study findings showed that the C_t/C_0 level in the designed experiments varied between 0.36581 and 0.91874. Among the recorded findings, the minimum C_t/C_0 value corresponds to experiment number 7, with an adsorbent mass of 0.016 g, at a pH level of 6, and a contact time of 60 min. The statistical analysis indicates that the adsorbent mass significantly affects the adsorbent pollutant ($p<0.05$). No significant correlation was observed between pH and adsorption mass ($p>0.05$) as well as between contact time and adsorption mass ($p>0.05$). On the other hand, as is known, mesoporous materials have a substantial surface area, thereby increasing their capacity to adsorb gases, liquids, hazardous heavy metals, and dyes. This feature makes them very efficient for adsorption-based applications. Then, since the SnSe adsorbent has a mesoporous structure with a high surface area, the mass of nanostructures can be a determining factor in adsorption efficiency [19, 20]. The linear model considered was significant, as evidenced by a model F-value of 6.75 and a p-value of 0.0139. The mathematical equation of this significant linear model obtained from the results can be expressed as follows:

$$^{C_t}/_{C_0} = +1.261 - 32.863 \times (\text{Adsorbent mass in g}) - 0.030 \times (\text{pH}) - 0.0003 \times (\text{Time in min})$$

Figure 2a shows the contour plot illustrating the relationship between the C_t/C_0 ratio, adsorbent mass (g), pH levels, and contact time of 35 min. The contour plot illustrates that the simultaneous increase in adsorbent mass and pH results in a decrease in the C_t/C_0 ratio, which is consistent with the findings of another research [21]. In a research study, the removal percentage of Chrysoidine R has been increased as the adsorbent mass and the solution pH were increased from 6 mg to 10 mg and 2 to 6, respectively [20, 21]. The findings are consistent with the results of the present study.

In general, as known, the adsorbent mass plays a crucial role in determining its capacity. With increasing adsorbent mass, the removal efficiency typically improves because more adsorption sites are available on the adsorbent's surface [2]. In addition, the initial pH of a solution significantly affects the capacity of the adsorbent. It plays a crucial role in water treatment because it affects both the ionization of the adsorbent molecules and the surface properties of the adsorbent. In addition, the adsorption efficiency is related to the chemistry of the dye in the solution as well as the ionization state of the functional groups of the adsorbent [2].

Figure 2b shows the contour plot that illustrates the relationship between adsorbent mass, contact time at pH 6 solution. The plot illustrates that the simultaneous increase in adsorbent mass and contact time leads to a decrease in the C_t/C_0 ratio, which is consistent with the findings of another research [21]. The comparison of two contour plots shows that a higher slope in the plot in **Figure 1a** corresponds to the significant effect of the simultaneous changes in pH levels and SnSe adsorbent mass on pollutant adsorption efficiency. Furthermore, the scatter plot presented in **Figure 2c** compared the model's predicted result with the actual results for the response. The minimal variance between the determined and actual values indicates the suitability of the linear model for predicting the C_t/C_0 ratio.

Table 2. Adsorption amounts of designed experiments

No. of Run	Adsorbent mass (g)	pH	Time (min)	C_t/C_0
1	0.006	4	35	0.91784
2	0.006	6	60	0.89165
3	0.006	6	10	0.8596
4	0.011	4	10	0.69889
5	0.016	8	35	0.54744
6	0.016	6	10	0.45982
7	0.016	6	60	0.36581
8	0.011	4	60	0.78707
9	0.006	8	35	0.82685
10	0.011	8	10	0.72781
11	0.016	4	35	0.80836
12	0.011	8	60	0.63711

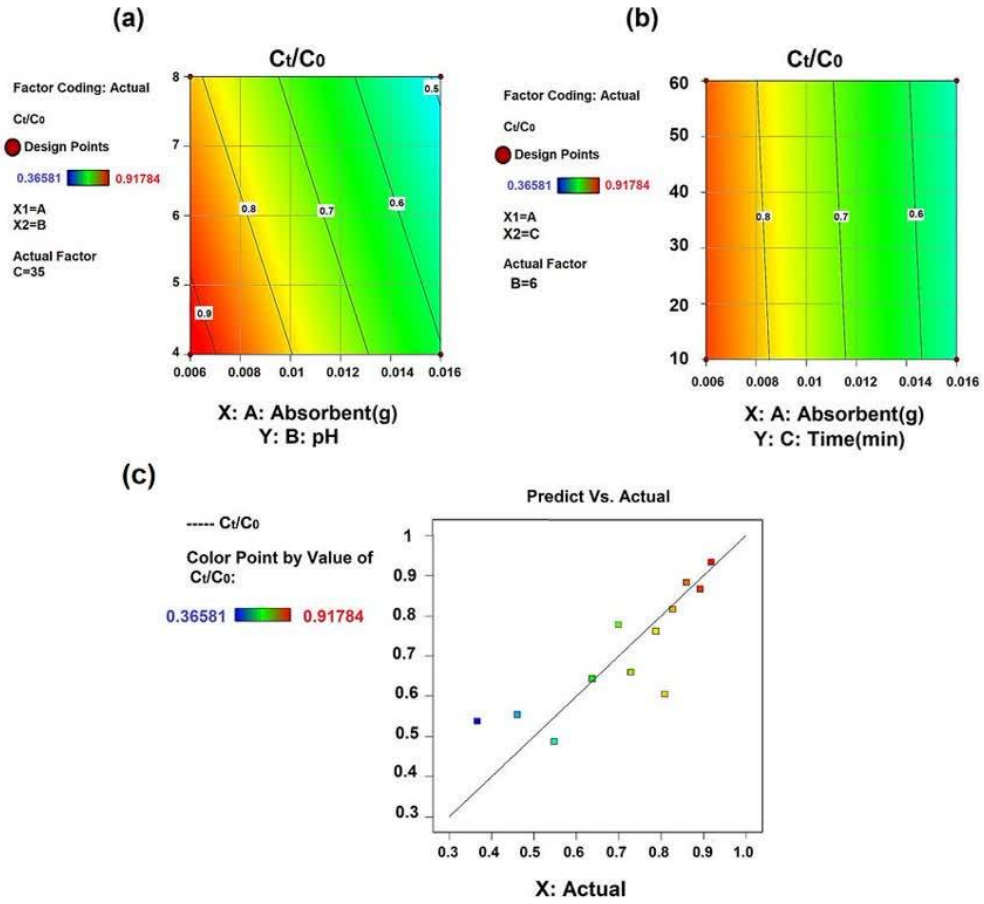

Figure 2. (**a**) contour plot of C_t/C_0 versus adsorbent mass (g) and pH levels; (**b**) contour plot of C_t/C_0 versus adsorbent mass (g) and contact time (min). (**c**) scatter plot comparing predicted values for the C_t/C_0 ratio with actual values using a linear model.

Figure 3a shows the one-factor effect plot, which suggest that the addition of adsorbent mass may lead to a significant decrease in the C_t/C_0 ratio. This increase in pollutant removal is related to the increase in the active adsorption sites due to the increase in the amount of mesoporous media and their better accessibility [21-23].

Figure 3b shows the one-factor effect plot, indicating that the increase in pH levels leads to a decrease in the C_t/C_0 ratio. As mentioned in the previous section, pH is a fundamental factor in the adsorption capacity of nanostructures. On the other hand, according to the results of XRD analysis, it is possible that excess Se^{2-} precursor oxidizes Sn^{2+} to Sn^{4+}, which leads to degenerate hole doping in the SnSe nanostructure. The introduction of a high concentration of holes (positive charge carriers) can increase the positive charge density on the surface of the SnSe nanostructures. In general, degenerate hole doping not only affects the electronic and optical properties of SnSe nanostructure but also has a significant effect on their surface charge and related interactions [24]. Therefore, it seems that with the increase in pH, due to the higher concentration of OH^- ions in the solution, the positive charges on the surface of the nanostructures can form electrostatic bonds with the OH^- ions present in the solution. This interaction leads to an improvement in the adsorption efficiency [25].

Figure 3c shows the one-factor effect plot, suggesting that passing time (min) may lead to a slight reduction in the C_t/C_0 ratio. The marginal degrease noted during the transition from 10 to 60 min indicates a significant adsorption of pollutants at the beginning of the process, meaning that the most of active sites on the mesoporous adsorbent are rapidly occupied by pollutants at the initial stage of adsorption. The initial adsorption of pollutants during the adsorption process is usually advantageous because it enhances the efficiency of pollutant removal, especially in settings such as wastewater treatment [5, 26].

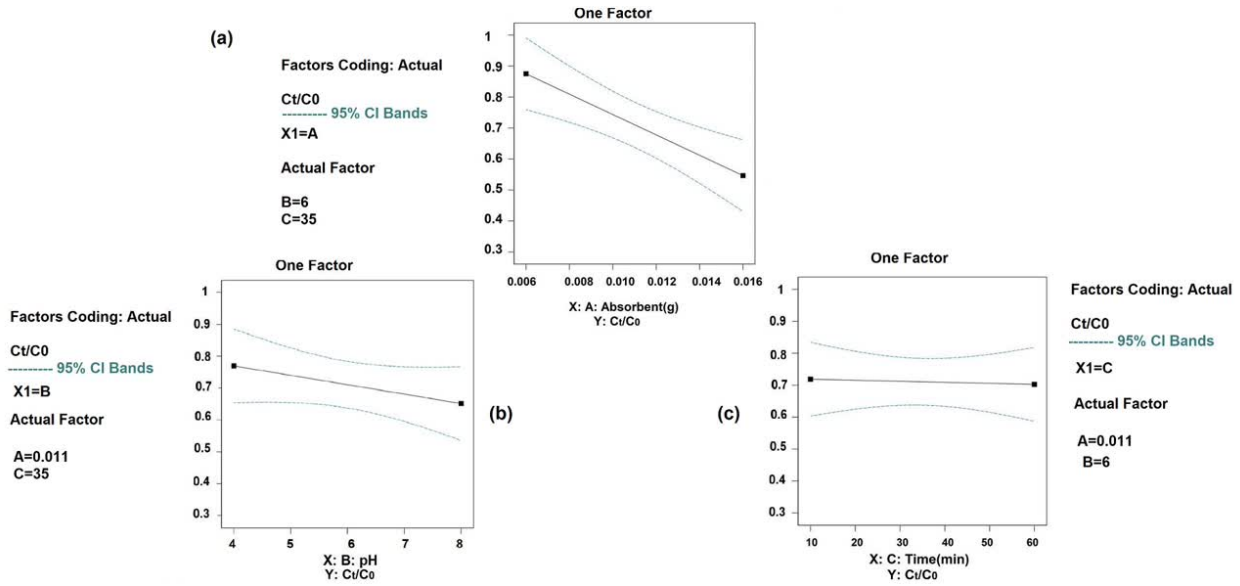

Figure 3. One-factor effect plot illustrating the ratio of C_t/C_0 versus (**a**) absorbent mass (g); (**b**) pH and (**c**) contact time (min) levels using a linear model.

Figure 4 illustrates the numerical optimization of design factors conducted based on experimental results. In the optimization, the suggested value for the C_t/C_0 ratio was determined to be 0.489246, which demonstrates a favorable adsorption rate. The optimal values for the factors corresponding to this predicted result are as follows; the mass of the mesoporous adsorbent is approximately 0.0157 g, the pH level is 8.0, and the contact time is 50 min. The optimal values of the factors were determined experimentally, and the C_t/C_0 ratio was determined to be 52% through measurement. Subsequently, the optimization accuracy was confirmed based on the minimum difference between the numerical optimization result and the experimental measurement.

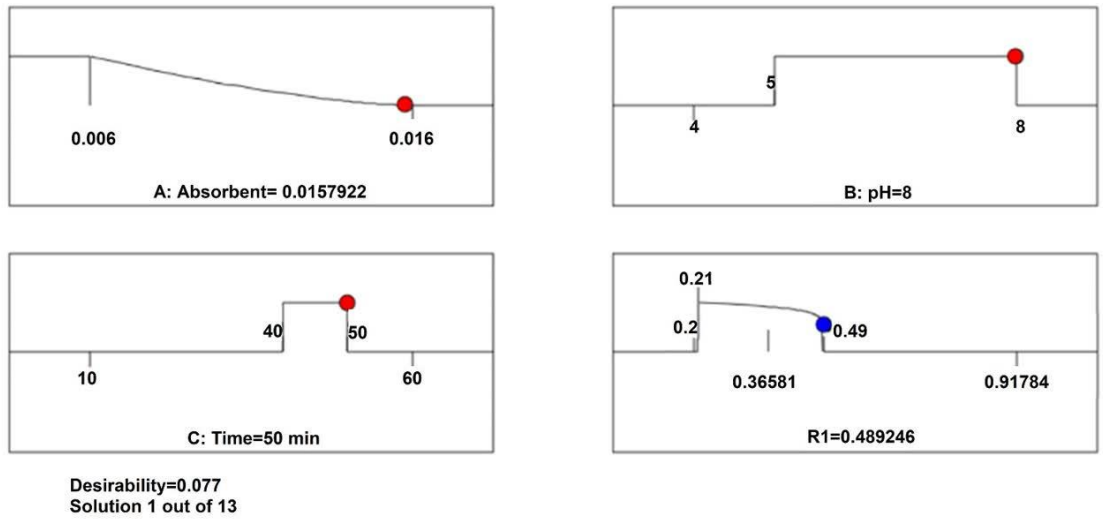

Figure 4. Numerical optimization of design factors based on experimental measurements for the C_t/C_0 ratio.

3.3. Investigation of the MB adsorption kinetics on SnSe nanostructures

In general, the selection of the optimal operating conditions in practical systems depends on the adsorption kinetics. The MB adsorption kinetics are determined by the physical and chemical properties of the adsorbent, which

subsequently affect the underlying adsorption mechanism. To evaluate the adsorption rate and investigate the kinetic mechanisms governing the adsorption process, the experimental data were analyzed using the pseudo-first-order and pseudo-second-order models. Equations (3) and (4) represent the pseudo-first kinetic model and pseudo-second kinetic model, respectively [12, 27-29].

$$\mathrm{Ln}(q_e - q_t) = \mathrm{Ln}q_e - \frac{k_1}{2.303}t \quad (3)$$

$$\frac{t}{q_t} = \frac{1}{k_2 q_e^2} + \frac{t}{q_e} \quad (4)$$

In these equations, q_e and q_t represent the equilibrium adsorption capacity (mgg^{-1}) and the adsorption capacity at a given time (mgg^{-1}), respectively. In addition, k_1 and k_2 represent the reaction rate constants for the first-order and second-order models, expressed in units of min^{-1} and L $mg^{-1}min^{-1}$, respectively.

It is noted that consistency between q_e obtained from the experiments (q_e(exp)) and q_e calculated from the relations (q_e(cal)) values are essential criteria for validating pseudo-first-order and pseudo-second-order kinetic models. **Figures 5a** and **b** show the effect of different contact times on MB removal percentage and adsorption capacity. It can be seen that the MB adsorption capacity on SnSe nanostructure reached equilibrium in about 10 min under conditions of an initial MB concentration of 10 ppm, pH 8.0, an adsorbent mass of 0.016 mg, and room temperature. It is clear that a large number of MB molecules are rapidly adsorbed onto SnSe nanoparticles in less than 5 min. This rapid adsorption is attributed to the very small size of the SnSe nanoparticles and their large effective surface area, as confirmed by BET analysis.

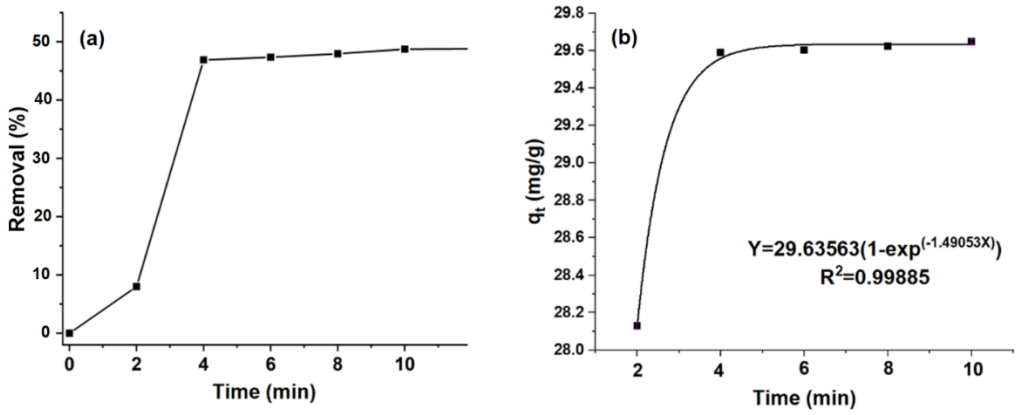

Figure 5. Effect of different contact time on: (**a**) MB removal percentage and (**b**) adsorption capacity.

For the pseudo-first-order kinetic model and pseudo-second-order kinetic, the linear plots of $Ln(q_e - q_t)$ versus time (t) and $\frac{t}{q_t}$ versus time (t) are plotted, respectively. The plots are shown in **Figures 6a** and **b**. The comparison of the pseudo-first-order model and pseudo-second-order model parameters, along with the q_e(cal) and q_e(exp) values obtained from the fitting results, are presented in **Table 3**. As observed, in the pseudo-first-order model, there is a notable discrepancy between the calculated q_e(cal) and experimental q_e(exp) values. Therefore, this kinetic model is not suitable for analyzing the adsorption kinetics on SnSe nanostructures, as indicated by an R^2 value of 0.84964.
On the other hand, the pseudo-second-order model results demonstrate that the q_e(cal) and q_e(exp) values are in perfect agreement. The R^2 values also show a stronger correlation, making the pseudo-second-order model more suitable for describing the MB adsorption on SnSe nanostructures.

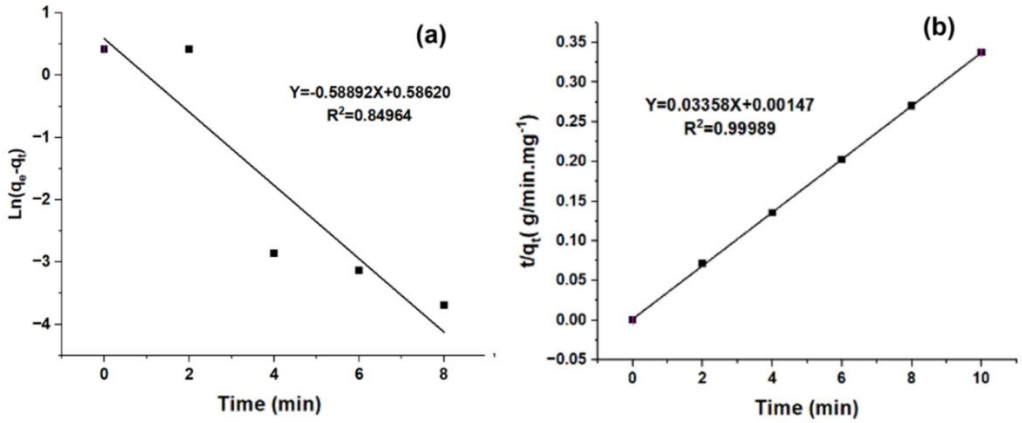

Figure 6. The MB adsorption kinetics on the SnSe nanostructures under optimal condition: (**a**) pseudo- first-order and (**b**) pseudo-second-order kinetic plots.

Table 3. Comparison of pseudo-first-order model and pseudo-second-order model parameters along with the q_e(cal) and q_e(exp) values, for the MB adsorption onto SnSe nanostructures.

Pseudo-first -order model				Pseudo-second -order model			
q_e(exp) (mgg^{-1})	q_e(cal) (mgg^{-1})	k_1(min^{-1})	R^2	q_e(exp) (mgg^{-1})	q_e(cal) (mgg^{-1})	k_2(min^{-1})	R^2
29.64769	1.79715	1.35628	0.84964	29.64769	29.77963	0.76709	0.99989

3.4. Adsorption isotherms

Adsorption isotherms are used to describe the interaction between the adsorbate and adsorbent materials. These isotherms also illustrate the adsorption capacity of the adsorbent. In the present study, the Langmuir and Freundlich isotherm models were applied to analyze the experimental data and describe the adsorption equilibrium between the solid and liquid phases. **Figure 7** shows the simulated data using the Langmuir and Freundlich isotherms for the SnSe nanostructures. The Langmuir isotherm model is based on the concept of a continuous monolayer of adsorbate molecules covering a homogeneous solid surface. Its linear form is expressed in Equation 5, and the plot of $\frac{1}{q_e}$ versus $\frac{1}{C_e}$ was used to determine the Langmuir correlation coefficients q_0 andK_L. These coefficients were estimated from the slope and intercept of the line, as shown in **Figure 7a.**

$$\frac{1}{q_e} = \frac{1}{q_0} + \frac{1}{K_L q_0 C_e} \quad (5)$$

where, K_L represents the Langmuir constant (L mg^{-1}) and $q_0$is the maximum adsorption capacity (mgg^{-1}).
The main characteristic of the Langmuir equation is a dimensionless constant called the equilibrium parameter (R_L) which can be calculated from equation 6.

$$R_L = \frac{1}{1+K_L \times C_0} \quad (6)$$

The value of R_L indicates the type of isotherm and the significant evidence about the nature of the adsorption. The MB adsorption process is favorable when $0 < R_L < 1$, unfavorable when $R_L > 1$, linear when $R_L = 1$, and reversible when $R_L = 0$. The results of the Langmuir isotherm analysis are summarized in **Table 4**. The value of $R_L = 0.16084$ and the correlation coefficient R^2=0.99927 indicate the favorable adsorption and fit of the data to the Langmuir isotherm [28, 30].

On the other hand, as is known, the Freundlich isotherm equation does not provide any prediction regarding the saturation of the adsorbent surface with the adsorbate. This isotherm is based on the concept of multilayer adsorption, characterized by a non-uniform and heterogeneous distribution of the adsorbed materials on the adsorbent surface and is defined as Equation 7 [31].

$$\mathrm{Lnq_e} = \mathrm{LnK_F} + \frac{1}{\mathrm{n}}\mathrm{LnC_e} \quad (7)$$

where, K_F represents the Freundlich constant, n is the heterogeneity factor and C_e is the equilibrium concentration (mgL^{-1}).

In **Figure 7b**, the plot of $\log q_e$ versus $\log C_e$ was used to determine the parameters K_F and $\frac{1}{n}$. The parameter of K_F ($mg\ g^{-1}$) represents the Freundlich correlation coefficient related to adsorption capacity, while $\frac{1}{n}$ (dimensionless) reflects the adsorption intensity. These values are obtained from the intercept on the vertical axis and the slope of the line, respectively. The MB adsorption is considered favorable when $0 < \frac{1}{n} < 1$, linear when $\frac{1}{n} = 1$, physical when $1 < \frac{1}{n}$, and chemical when $\frac{1}{n} < 1$. Irreversible adsorption occurs when $\frac{1}{n} = 0$. It is noteworthy that a smaller 1/n value indicates greater heterogeneity of the adsorbent used [28]. The results obtained from the Freundlich isotherm analysis, presented in **Table 4**, also show that based on the values of $\frac{1}{n}$ the adsorption process is favorable and occurs physically, suggesting that the adsorption process follows the Freundlich isotherm.

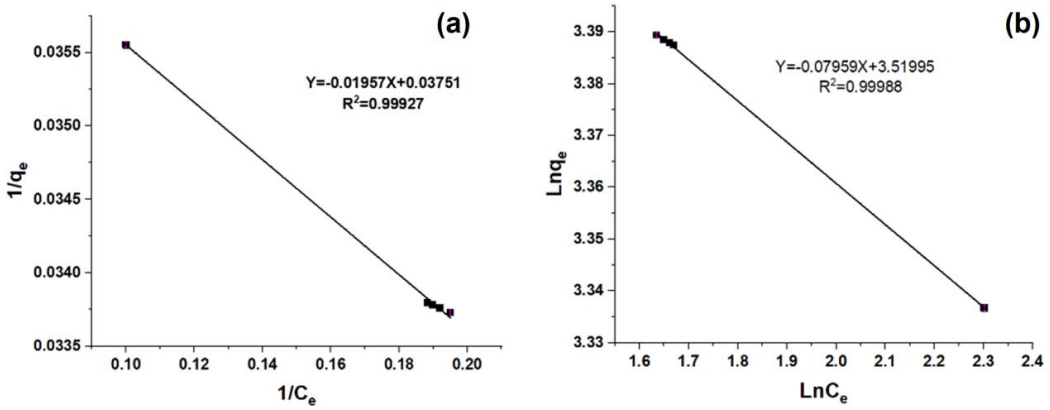

Figure 7. Linearization of (**a**) Langmuir and (**b**) Freundlich isotherm models.

Table 4. Parameters of Langmuir and Freundlich models of MB adsorption on SnSe nanostructures.

Langmuir constants				Freundlich constants			
$q_m(mgg^{-1})$	$K_L(Lmg^{-1})$	R_L	R^2	n	n^{-1}	$K_F(mg^{1-n}L^ng^{-1})$	R^2
26.65956	0.52173	0.16084	0.99927	26.65956	0.52173	0.16084	0.99988

4. Conclusions

In this study, the SnSe nanostructures were synthesized, characterized, and for the first time applied as adsorbents for the removal of MB dye from aqueous solutions. The synthesized SnSe exhibited high surface activity and favorable adsorption kinetics toward MB molecules. To optimize the adsorption parameters (pH, contact time, and adsorbent dosage), a set of 12 experiments was designed using response surface methodology (RSM) based on the Box-Behnken model. The optimal conditions for maximum MB removal were found at pH 8, contact time of 50 minutes, and adsorbent mass of 0.0157 g. Kinetic analysis showed that the adsorption followed a pseudo-second-order model with a rapid initial uptake, achieving 49% dye removal within 10 minutes. This fast adsorption rate is considered a significant advantage for real-world water treatment applications. While optimal conditions yielded the highest efficiency, it is important to note that favorable adsorption performance was also observed under varying conditions, particularly when the effects of parameter interactions were properly balanced. For instance, at lower pH levels, the adsorption rate decreased; however, this could be compensated by increasing the adsorbent dosage.

Isotherm modeling indicated that the Langmuir isotherm provided a better fit to the equilibrium data compared to other models, with a high correlation coefficient. These results suggest that the MB adsorption onto SnSe

nanostructures proceeds via a favorable and predominantly physical mechanism. Overall, this study demonstrates the potential of SnSe nanostructures as promising, fast-acting, and cost-effective adsorbents for dye removal from wastewater.

Authors' contributions

Marzieh Khademalrasool: Writing–review & editing, Writing–original draft, Visualization, Validation, Supervision, Resources, Project administration, Methodology, Investigation, Funding acquisition, Formal analysis, Data curation, Conceptualization. **Elham Kharatzadeh:** Writing–review & editing, Writing–original draft, Visualization, Validation, Supervision, Resources, Methodology, Investigation, Formal analysis, Data curation, Conceptualization. **Atefeh Pourjahed:** Writing – review & editing, Writing– original draft, Visualization, Validation, Supervision, Software, Resources, Methodology, Investigation, Formal analysis, Data curation, Conceptualization.

Declaration of competing interest

The authors declare that they have no known competing financial interests or personal relationships that could have appeared to influence the work reported in this paper.

Funding

This paper received no funding.

Acknowledgment

The authors acknowledge the Jundi-Shapur University of Technology of Dezful for supporting this research (project code: 403-2-500-01).

Data availability

Data will be made available on request.

References

[1] K.B. Tan, M. Vakili, B.A. Horri, P.E. Poh, A.Z. Abdullah, B. Salamatinia, Adsorption of dyes by nanomaterials: recent developments and adsorption mechanisms, Sep. Purif. Technol. 150 (2015) 229–242.
DOI: https://doi.org/10.1016/j.seppur.2015.07.009

[2] E.N. Zare, A. Motahari, M. Sillanpää, Nanoadsorbents based on conducting polymer nanocomposites with main focus on polyaniline and its derivatives for removal of heavy metal ions/dyes: a review, Environ. Res. 162 (2018) 173–195.
DOI: https://doi.org/10.1016/j.envres.2017.12.025

[3] I. Ali, New generation adsorbents for water treatment, Chem. Rev. 112 (2012) 5073–5091.
DOI: https://doi.org/10.1021/cr300133d

[4] M. Channegowda, Recent advances in environmentally benign hierarchical inorganic nano-adsorbents for the removal of poisonous metal ions in water: a review with mechanistic insight into toxicity and adsorption, Nanoscale Adv. 2 (2020) 5529–5554.
DOI: https://doi.org/10.1039/D0NA00580E

[5] J. Vievard, A. Alem, A. Pantet, N.-D. Ahfir, M.G. Arellano-Sánchez, C. Devouge-Boyer, M. Mignot, Bio-based adsorption as ecofriendly method for wastewater decontamination: a review, Toxics 11 (2023) 404.
DOI: https://doi.org/10.3390/toxics11050404

[6] E. Kharatzadeh, M. Khademalrasool, R. Yousefi, Enhanced visible-light photovoltaic and photocatalytic performances of SnSe1-xSx nanostructures, Surf. Interfaces 30 (2022) 101916.
DOI: https://doi.org/10.1016/j.surfin.2022.101916

[7] E. Kharatzadeh, S.R. Masharian, R. Yousefi, Comparison of the photocatalytic performance of S-SnSe/GO and SnSe/S-GO nanocomposites for dye photodegradation, Mater. Res. Bull. 135 (2021) 111127.
DOI: https://doi.org/10.1016/j.materresbull.2020.111127

[8] W. Shi, M. Gao, J. Wei, J. Gao, C. Fan, E. Ashalley, H. Li, Z. Wang, Tin selenide (SnSe): growth, properties, and applications, Adv. Sci. 5 (2018) 1700602.
DOI: https://doi.org/10.1002/advs.201700602

[9] V.A. Sakkas, M.A. Islam, C. Stalikas, T.A. Albanis, Photocatalytic degradation using design of experiments: a review and example of the Congo red degradation, J. Hazard. Mater. 175 (2010) 33–44.
DOI: https://doi.org/10.1016/j.jhazmat.2009.09.118

[10] C. Sahoo, A. Gupta, Optimization of photocatalytic degradation of methyl blue using silver ion doped titanium dioxide by combination of experimental design and response surface approach, J. Hazard. Mater. 215 (2012) 302–310.
DOI: https://doi.org/10.1016/j.jhazmat.2012.02.072
[11] A.W. Skinner, A.M. DiBernardo, A.M. Masud, N. Aich, A.H. Pinto, Factorial design of experiments for optimization of photocatalytic degradation of tartrazine by zinc oxide (ZnO) nanorods with different aspect ratios, J. Environ. Chem. Eng. 8 (2020) 104235.
DOI: https://doi.org/10.1016/j.jece.2020.104235
[12] A. Mehrdoost, R.J. Yengejeh, M.K. Mohammadi, A. Haghighatzadeh, A.A. Babaei, Adsorption removal and photocatalytic degradation of azithromycin from aqueous solution using PAC/Fe/Ag/Zn nanocomposite, Environ. Sci. Pollut. Res. 29 (2022) 33514–33527.
DOI: https://doi.org/10.1007/s11356-021-17889-2
[13] E. Kharatzadeh, S.R. Masharian, R. Yousefi, The effects of S-doping concentration on the photocatalytic performance of SnSe/S-GO nanocomposites, Adv. Powder Technol. 32 (2021) 346–357.
DOI: https://doi.org/10.1016/j.apt.2020.12.019
[14] H. Ju, K. Kim, D. Park, J. Kim, Fabrication of porous SnSeS nanosheets with controlled porosity and their enhanced thermoelectric performance, Chem. Eng. J. 335 (2018) 560–566.
DOI: https://doi.org/10.1016/j.cej.2017.10.163
[15] S. Patel, S. Chaki, P. Vinodkumar, Effect of sulphur doping in SnSe single crystals on thermoelectric power, Mater. Res. Express 6 (2019) 085910.
DOI: https://doi.org/10.1088/2053-1591/ab23ee
[16] M.A. Dar, D. Govindarajan, G.N. Dar, Facile synthesis of SnS nanostructures with different morphologies for supercapacitor and dye-sensitized solar cell applications, J. Mater. Sci.: Mater. Electron. 32 (2021) 20394–20409.
DOI: https://doi.org/10.1007/s10854-021-06545-7
[17] C. Lievens, D. Mourant, M. He, R. Gunawan, X. Li, C.Z. Li, An FT-IR Spectroscopic Study of Carbonyl Functionalities in Bio-oils, Fuel 90 (2011) 3417–3423.
DOI: https://doi.org/10.1016/j.fuel.2011.06.042
[18] M. Thommes, K. Kaneko, A.V. Neimark, J.P. Olivier, F. Rodriguez-Reinoso, J. Rouquerol, K.S. Sing, Physisorption of gases, with special reference to the evaluation of surface area and pore size distribution (IUPAC Technical Report), Pure Appl. Chem. 87 (2015) 1051–1069.
DOI: https://doi.org/10.1515/pac-2014-1117
[19] R. Xiao, Y. Zhang, K. Long, Z. Xiong, J. Zhang, Y. Zhao, Multiscale Investigation of 3D Morphology SnSe2 for Mercury Removal from Flue Gas: Experimental and Simulation Studies, Energy Fuels 38 (2024) 16610–16621.
DOI: https://doi.org/10.1021/acs.energyfuels.4c02225
[20] A.E. Mahdi, N.S. Ali, H.S. Majdi, T.M. Albayati, M.A. Abdulrahman, D.J. Jasim, K.R. Kalash, I.K. Salih, Effective adsorption of 2-nitroaniline from wastewater applying mesoporous material MCM-48: equilibrium, isotherm, and mechanism investigation, Desalin. Water Treat. 300 (2023) 120–129.
DOI: https://doi.org/10.5004/dwt.2023.29515
[21] M. Zbair, H.A. Ahsaine, Z. Anfar, Porous Carbon by Microwave Assisted Pyrolysis: An Effective and Low-cost Adsorbent for Sulfamethoxazole Adsorption and Optimization Using Response Surface Methodology, J. Clean. Prod. 202 (2018) 571–581.
DOI: https://doi.org/10.1016/j.jclepro.2018.08.155
[22] D. Flores, C.M.R. Almeida, C.R. Gomes, S.S. Balula, C.M. Granadeiro, Tailoring of mesoporous silica-based materials for enhanced water pollutants removal, Molecules 28 (2023) 4038.
DOI: https://doi.org/10.3390/molecules28104038
[23] P. Zhang, M. He, W. Teng, F. Li, X. Qiu, K. Li, H. Wang, Ordered mesoporous materials for water pollution treatment: Adsorption and catalysis, Green Energy Environ. 9 (2024) 1239–1256.
DOI: https://doi.org/10.1016/j.gee.2022.10.008
[24] W.J. Mir, A. Sharma, D.R. Villalva, J. Liu, M.A. Haque, S. Shikin, D. Baran, The ultralow thermal conductivity and tunable thermoelectric properties of surfactant-free SnSe nanocrystals, RSC Adv. 11 (2021) 28072–28080.
DOI: https://doi.org/10.1039/D1RA03804C
[25] X. Cai, J. He, L. Chen, K. Chen, Y. Li, K. Zhang, Z. Jin, J. Liu, C. Wang, X. Wang, A 2D-g-C3N4 nanosheet as an eco-friendly adsorbent for various environmental pollutants in water, Chemosphere 171 (2017) 192–201.
DOI: https://doi.org/10.1016/j.chemosphere.2016.12.073
[26] R. Rashid, I. Shafiq, P. Akhter, M.J. Iqbal, M. Hussain, A State-of-the-art Review on Wastewater Treatment Techniques: The Effectiveness of Adsorption Method, Environ. Sci. Pollut. Res. 28 (2021) 9050–9066.
DOI: https://doi.org/10.1007/s11356-021-12395-x
[27] M. Batvandi, A. Haghighatzadeh, B. Mazinani, J. Dutta, Visible-light-driven photocatalysis with Z-scheme Ag3PO4@ N-GQDs@ g-C3N4 nano/hetero-junctions, Appl. Phys. A 128 (2022) 853.
DOI: https://doi.org/10.1007/s00339-022-06001-1
[28] S. Gupta, B. Babu, Modeling, simulation, and experimental validation for continuous Cr (VI) removal from aqueous solutions using sawdust as an adsorbent, Bioresour. Technol. 100 (2009) 5633–5640.
DOI: https://doi.org/10.1016/j.biortech.2009.06.024

[29] M. Vigdorowitsch, A. Pchelintsev, L. Tsygankova, E. Tanygina, Freundlich Isotherm: An Adsorption Model Complete Framework, Appl. Sci. 11 (2021) 8078.
DOI: https://doi.org/10.3390/app11178078
[30] G. Bayramoglu, I. Gursel, Y. Tunali, M.Y. Arica, Biosorption of phenol and 2-chlorophenol by Funalia trogii pellets, Bioresour. Technol. 100 (2009) 2685–2691.
DOI: https://doi.org/10.1016/j.biortech.2008.12.041
[31] M. Vigdorowitsch, A. Pchelintsev, L. Tsygankova, & E. Tanygina, Freundlich isotherm: An adsorption model complete framework. Appl. Sci., 11(17) (2021) 8078.
DOI: https://doi.org/10.3390/app11178078